JOURNAL OF SOLID STATE CHEMISTRY **136,** 151–159 (1998)
ARTICLE NO. SC977663

Single-Crystal Studies of the Chevrel-Phase Superconductor $La_xMo_6Se_8$

I: Correlation between T_c and the Interatomic Distances

F. Le Berre,[1] O. Peña,[2] C. Perrin, and M. Sergent

Chimie du Solide et Inorganique Moléculaire, UMR CNRS 6511, Université de Rennes I, 35042 Rennes Cedex, France

and

R. Horyń and A. Wojakowski

Institute of Low Temperature and Structure Research, Polish Academy of Sciences, 50 950 Wroclaw 2, Poland

Received October 9, 1996; in revised form October 9, 1997; accepted October 14, 1997

We report, for the first time in the literature, crystal structure studies of rare-earth-based Chevrel-phase selenides of formulae $La_xMo_6Se_8$ with variable contents (x) of lanthanum. Single crystals were grown from off-stoichiometric mixtures that had been melted and slowly cooled from about 1675°C. The origin site of the rhombohedral lattice may present a considerable deficiency in the lanthanum occupancy, whereas no vacancies were found in the Mo_6Se_8 sublattice. The superconducting temperature of this phase depends strongly on the lanthanum concentration, as we previously reported for powder samples. From the crystal structure data obtained for three crystals with different lanthanum contents, a clear correlation was established between T_c and the lanthanum occupancy at the origin site. The critical temperature varied from 9.4 to 11.0 K for $x = 0.839(2)$ to $x = 0.9412(2)$, respectively, the lanthanum contents being derived from structural data taken on the same single crystals. Lattice constants, positional parameters, and interatomic distances are presented, and their respective variations are discussed in terms of geometrical effects and charge transfer phenomena. A full comparison is made with the corresponding rare-earth molybdenum sulfides $RE Mo_6S_8$. Basic physical properties, i.e., electrical resistivity, ac susceptibility, and dc magnetization, are presented in an accompanying paper; they confirm that $LaMo_6Se_8$ is an extremely high-field superconductor.

1. INTRODUCTION

Magnetic superconductors are one of the most challenging problems in solid-state physics. True coexistence of both superconductivity and long-range magnetic interactions became possible only when two fairly independent crystallographic networks were fashioned into a three-dimensional lattice. The discovery in the mid 1970s of two families of ternary compounds [the Chevrel phases $RE Mo_6X_8$ and the rhodium borides $RE Rh_4B_4$ (X = S, Se; RE = rare earths) (1–3)] prompted experimentalists and theoreticians to work actively in this field for more than a decade. Later, the research on high-T_c superconductors slowed down the pace on this exciting subject, although weak long-range interactions were also found in some of the high-T_c materials [$RE Ba_2Cu_3O_x$, RE = Gd, Dy, Ho, Er; $RE_{2-x}Ce_xCuO_4$, RE = Sm, Nd; etc. (4–6)]. A recent revival of this question happened after the discovery of the quaternary intermetallic compounds $RE Ni_2B_2C$ (7, 8), where superconductivity and magnetic order also coexist.

Proper and careful sample preparation is absolutely necessary, not only because of stoichiometric considerations but also in order to investigate the intrinsic properties related to their crystal structure. This is extremely important in the case of coexistence phenomena since secondary phases found in minute amounts may, sometimes, hinder the essential properties of the desired compound. Obviously, single crystals constitute the ultimate stage in sample preparation, but appropriate growth techniques for ternary and quaternary materials are sometimes difficult to accomplish.

In the case of Chevrel phases, the presence of a chalcogen sublattice generally leads to a peritectic character of the melting. In addition, high melting points for rare-earth compounds (9, 10), together with their high reactivity and tendency to oxidize, make the crystal growth of these materials complex and difficult. As a consequence, studies

[1] Part of the thesis work presented by F. Le Berre at the Université de Rennes I, France, 1996. Present address: Université du Maine, 72017 Le Mans, France.

[2] To whom correspondence should be addressed.

0022-4596/98 $25.00

of single crystals of rare-earth-based Chevrel phases $RE\mathrm{Mo}_6X_8$ were delayed until the mid 1980s. Since then, crystals of almost all the sulfide series $RE\mathrm{Mo}_6\mathrm{S}_8$ have been grown (10) and their properties studied (for a full review, see ref. 11).

The growth of the selenide series $RE\mathrm{Mo}_6\mathrm{Se}_8$ presents additional difficulties, especially due to the existence of a binary phase $\mathrm{Mo}_6\mathrm{Se}_8$ ($\mathrm{Mo}_3\mathrm{Se}_4$), isostructural with the ternary 1 : 6 : 8 phase and with quite similar superconducting properties [e.g., $T_c = 6.45\,\mathrm{K}$ for $\mathrm{Mo}_3\mathrm{Se}_4$ (12); $6\,\mathrm{K} < T_c < 12\,\mathrm{K}$ for $RE\mathrm{Mo}_6\mathrm{Se}_8$ (2)]. First trials of crystal growth of these compounds led to sandwich-like materials with alternate layers of each phase growing simultaneously (13). Their superconducting properties were explained on the basis of proximity effects, whereas their magnetic properties resembled those of a ternary phase with a hypothetical highly deficient rare-earth sublattice (of the order of 50% or less) (13–15). Such deficiency is far from reality in view of the well-defined boundaries of the Chevrel-phase compounds $RE\mathrm{Mo}_6X_8$ [for instance, in the La–Mo–Se system investigated at 1200°C, the rare-earth concentration ranges from ~5 to 7.5 at.%, which gives a lower limit of about 75% rare-earth occupancy (16)].

Recently, our modified approach to the crystal growth of these selenides has led to single-phase materials of compositions close to the ideal one (1 : 6 : 8). The modified method consisted mainly of a 24-hr presintering of off-stoichiometric compositions followed by melting and slow cooling (16, 17). The resulting crystals cover only a small composition domain, compared with the rather large domain of homogeneity found at 1200°C in the case of the lanthanum representative (16). With these modifications, and contrary to our previous trials, no traces of the binary phase $\mathrm{Mo}_3\mathrm{Se}_4$ were found cocrystallizing with the ternary compound. Properties correlate well with the rare-earth content but no detailed analysis has been done up to now on the relations between the crystallographic parameters and the physical behavior.

To make a detailed correlation between the interatomic distances, the rare-earth content, and the superconducting properties, we present herein a full work on the structure refinement of three $\mathrm{La}_x\mathrm{Mo}_6\mathrm{Se}_8$ single crystals, which have been well characterized through their superconducting temperatures and their rare-earth occupancies. An accompanying paper describes some basic physical (magnetic, transport, and superconducting) properties (18).

2. EXPERIMENTAL

2.1. Materials Elaboration

MoSe_2, molybdenum metal, and lanthanum selenide, all in powder form, were used as starting materials. Molybdenum diselenide was prepared by direct synthesis of the constituent elements (purities, 99.99%) after reduction of the molybdenum powder in a hydrogen stream at 850°C for 4 hr.

Lanthanum selenide was prepared by direct reaction between the metal (purity, 99.9%) and the chalcogen in a dual-chamber quartz tube, with the lanthanum pieces placed in an alumina boat to avoid direct contact with the silica walls. The reaction temperature was slowly increased until full consumption of selenide vapors. Exact stoichiometry of the final product was calculated after burning a small portion of the selenide and transforming it into $\mathrm{La}_2\mathrm{O}_3$.

Six to eight grams of pellets of composition $\mathrm{La}_{0.15}\mathrm{Mo}_{0.30}\mathrm{Se}_{0.55}$ was prepared from these starting materials. This composition was chosen to be slightly above the binary line [$\mathrm{LaMo}_6\mathrm{Se}_8$–$\mathrm{La}_2\mathrm{Se}_3$] within the three-phase field [$\mathrm{MoSe}_2 + \mathrm{La}_x\mathrm{Mo}_6\mathrm{Se}_8 + \mathrm{La}_2\mathrm{Se}_3$]. Pellets were then sealed inside a molybdenum crucible that was previously outgassed at high temperature under a secondary vacuum. No sample-protecting $\mathrm{Al}_2\mathrm{O}_3$ crucible was placed inside. Prior to melting, the pellets were presintered for 24 hr at 1200°C to reach the desired starting composition mentioned earlier. Crystal growth was then performed in the same furnace (high-temperature graphite resistor) using a well-defined temperature profile and reaching a maximum temperature of about 1675°C.

The crystal growth process is schematically illustrated in Fig. 1. The initial charge, of nominal formula $\mathrm{La}_{0.15}\mathrm{Mo}_{0.30}\mathrm{Se}_{0.55}$, shifts its overall composition due to the decomposition and loss of Se via secondary reaction of its vapor with the molybdenum-crucible walls. When such a charge is slowly cooled, it will produce single crystals of the lanthanum-based Chevrel phase. However, due to the fact that these crystals represent the case of a peritectic phase exhibiting a wide domain of existence, such crystals will show variable contents of lanthanum ($\mathrm{La}_x\mathrm{Mo}_6\mathrm{Se}_8$), with x increasing as the temperature decreases. Figure 1 shows, for instance, crystals 1, 2, and 3 studied in this work, which are released from a liquid phase of composition L_1, L_2, and L_3, respectively. The crystallization will finish at ~1620°C, and the resulting product will be mainly composed of a mixture of crystals of the ternary Chevrel phase and the lanthanum selenide.

The binary lanthanum selenide was then dissolved using a mixture of hydrochloric acid and ethyl alcohol (~20 vol% HCl), thus obtaining the crystals of the expected phase. Further cleaning and trimming were performed under an optical microscope before purity and quality were checked on a scanning electron microscope equipped with an energy-dispersive X-ray spectrometer (EDS). X-ray powder patterns were obtained at different stages of the sample preparation, including crushed polycrystals, to confirm the phase relations obeyed by these ternary systems.

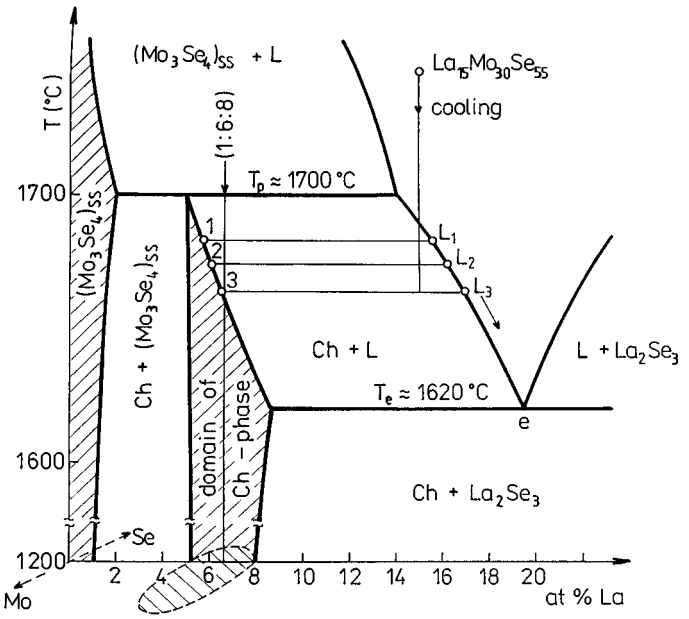

FIG. 1. Schematic illustration of the inhomogeneous distribution of La in single crystals of the $La_xMo_6Se_8$ (Ch) phase produced by melting and slow cooling of an off-stoichiometric composition $La_{0.15}Mo_{0.30}Se_{0.55}$. Points 1, 2, and 3 represent the chemical compositions of the single crystals studied in this work, created within the field of primary crystallization of the $La_xMo_6Se_8$ phase; L_1, L_2, and L_3 represent the corresponding liquid phase and its variation versus temperature.

2.2. Crystal Structure Analysis and Refinement

Three single crystals for structural refinement were selected according to their superconducting temperatures T_c (see results section). Since one of the main goals of this work was to unambiguously correlate the interatomic distances and lanthanum occupancies to the T_c values, the structure analysis *had to be performed on the same crystals* measured on the mutual-inductance bridge. As a result, the dimensions of the crystals were rather large compared to common standards (Table 1), which led us to take several precautions for the absorption corrections, as described in the following.

The crystal structure was analyzed at room temperature using an automatic X-ray Enraf-Nonius CAD-4 diffractometer. The cell parameters were refined by least-squares fits of 25 reflections ($5^\circ < \theta < 15^\circ$). Monochromatic (graphite monochromator) Mo$K\alpha$ radiation ($\lambda = 0.71069$ Å) was used, and a ω–2θ scan technique was applied in half of the reciprocal space ($\theta < 45^\circ$). Three standard reflections were monitored every 60 min, with no decay in intensities. Specific data collection conditions for each of the three single crystals are given in Table 1. Cell parameters of the rhombohedral and hexagonal lattices together with the individual superconducting critical temperatures T_c are given in Table 2. Intensities were corrected for the Lorentz–polarization factor. Gaussian absorption corrections were applied using the CRYSTAL program (19). The corresponding minimum and maximum transmission factors are reported in Table 1.

All calculations were performed using the MOLEN program implemented on a Microvax 3100 minicomputer. The crystal structure was refined in space group $R\bar{3}$ and it was assumed to be similar to that known for typical Chevrel-phase structures with large cations, for example, $PbMo_6S_8$ or $REMo_6S_8$ (20, 21): the Mo and Se(1) atoms were placed in 6*f* positions, Se(2) was placed in the 2*c* position, and the lanthanum atom was fixed in the 1*a* atomic position. All these positions were first assumed to be fully occupied. During refinement, electron deficiencies were observed at the lanthanum sites, whereas the occupancies at the other positions did not differ significantly from unity. On the final refinements, the atomic positions, the lanthanum occupancies and the anisotropic thermal factors for each of the three crystals converged toward the values reported in Tables 3–5. A final difference map of the electronic density did not show any residual peaks above 1 e $Å^{-3}$, meaning that there is no other site occupied by the lanthanum atoms. Additional information (*hkl* structural factors etc.) may be obtained upon request.

3. RESULTS

3.1. Choice of Crystals for Structure Refinement

Several groups of $La_xMo_6Se_8$ crystals were measured inductively by using a mutual-inductance bridge working at low frequency (119 Hz) and low field ($h_{ac} \sim 10$ mOe). Large and inhomogeneous transitions were observed, spread over almost 3 K, suggesting several superconducting phases or just one phase with different concentrations of lanthanum in the crystals. At a smaller scale, we observed that even one single specimen behaved similarly, although no spurious phases could be detected in an EDS–SEM analysis.

This observation led us to conclude that lanthanum was distributed inhomogeneously along the crystal during its formation, as the composition of the liquid phase changed with temperature. The resulting product was mainly composed of crystals having a concentration gradient (leading to broad superconducting transitions, such as the one shown in Fig. 2a, for each individual specimen) but also of some single crystals presenting quite narrow transitions ($\Delta T_c \leq 0.2$ K) such as those shown in Fig. 2b.

Three crystals (numbered 1, 2, and 3 in Fig. 2b) having well-defined inductive transitions at T_c (respectively 9.40(5), 10.25(5), and 11.00(5) K) were chosen for structural refinement. Their crystalline quality was checked by Weissenberg and/or four-circle-diffractometry techniques prior to data collection for crystal structure refinement. Their lattice parameters correlated well with the superconducting

TABLE 1
Crystal Data Collection (Crystals 1, 2, and 3 Defined in Figs. 1 and 2)

	$La_{0.84}Mo_6Se$	$La_{0.88}Mo_6Se_8$	$La_{0.94}Mo_6Se_8$
Crystal size (mm^3)	$0.34 \times 0.24 \times 0.24$	$0.34 \times 0.26 \times 0.23$	$0.28 \times 0.28 \times 0.18$
Linear absorption factors (mm^{-1})	32.55	32.52	32.46
Data collection			
	$0 < h < 13$	$-13 < h < 13$	$0 < h < 13$
	$0 < k < 13$	$0 < k < 13$	$0 < k < 13$
	$-13 < l < 13$	$0 < l < 13$	$-13 < l < 13$
Measured reflections	2871	2871	2873
Independent reflections (with $I > \sigma(I)$)	1582	1565	1563
R_{int}	0.02	0.03	0.02
Structure determination			
Gaussian absorption correction	$T_{min} = 0.0026$	$T_{min} = 0.0056$	$T_{min} = 0.0051$
	$T_{max} = 0.058$	$T_{max} = 0.057$	$T_{max} = 0.073$
Independent reflections (with $I > 3\sigma(I)$)	1446	1445	1464
Bad reflections eliminated[a]	5	5	10
Refined parameters	26	26	26
Unweighted agreement factor R	0.036	0.039	0.042
Weighted agreement factor R_w	0.049	0.051	0.052
w	$4F_o^2/[\sigma^2 F_o^2 + (0.06F_o^2)]$	$4F_o^2/[\sigma^2 F_o^2 + (0.06F_o^2)]$	$4F_o^2/[\sigma^2 F_o^2 + (0.07F_o^2)]$
S	1.28	1.31	1.27
$\Delta\rho_{max}$(e $Å^{-3}$)	0.44	0.39	0.14
Extinction coefficient	$1.17(6) \times 10^{-6}$	$1.15(6) \times 10^{-6}$	$1.57(6) \times 10^{-6}$

[a] The five bad reflections correspond to the worst reflections of the data collection and do not correspond to any special *hkl* values having some influence on the space group.

temperatures, the largest cell volume corresponding to the highest T_c (Table 2 and Fig. 3).

3.2. Crystal Structure

3.2.1. Description

All lanthanum–molybdenum–selenide single crystals studied in this work presented the same crystal structure ($R\bar{3}$ space group) as all the Chevrel-phase compounds with large cations, in particular rare earths. The structure is described by Mo_6Se_8 units and a pseudocubic origin site occupied by the lanthanum atom, stacked along a threefold axis in a rhombohedral unit cell, as shown in Fig. 4. The

TABLE 2
Crystallographic Data and Superconducting Temperature for $La_xMo_6Se_8$[a]

	$La_{0.84}Mo_6Se_8$	$La_{0.88}Mo_6Se_8$	$La_{0.94}Mo_6Se_8$
M (g/mol)	1324.00	1329.60	1338.00
a_r (Å)	6.7551(6)	6.7577(9)	6.7618(3)
α_r (deg)	88.68(1)	88.62(2)	88.60(1)
V_r ($Å^3$)	308.0(1)	308.3(2)	308.89(4)
a_h (Å)	9.442(2)	9.441(2)	9.4451(5)
c_h (Å)	11.967(2)	11.983(6)	11.995(1)
V_h ($Å^3$)	924.0(2)	925.0(5)	926.7(1)
ρ_{cal} (g/cm^3)	7.14	7.16	7.19
T_c (K)	9.40(5)	10.25(5)	11.00(5)

[a] Crystal system, trigonal, Space group, $R\bar{3}$; $Z = 1$ (rhombohedral unit cell).

TABLE 3
Site Multiplicities and Total Atomic Occupancies

	Atom	Position	Site multiplicity	Refined multiplicity	Atomic occupancy[a]
$La_{0.84}Mo_6Se_8$	La	1*a*	0.167	0.1398(4)	0.839(2)
	Mo	6*f*	1	1	1
	Se(1)	6*f*	1	1	1
	Se(2)	2*c*	0.333	0.333	1
$La_{0.88}Mo_6Se_8$	La	1*a*	0.167	0.1470(4)	0.882(2)
	Mo	6*f*	1	1	1
	Se(1)	6*f*	1	1	1
	Se(2)	2*c*	0.333	0.333	1
$La_{0.94}Mo_6Se_8$	La	1*a*	0.167	0.1568(4)	0.941(2)
	Mo	6*f*	1	1	1
	Se(1)	6*f*	1	1	1
	Se(2)	2*c*	0.333	0.333	1

[a] The more realistic results 0.84(1), 0.88(1), and 0.94(1) are used in the text for crystals 1, 2, and 3, respectively.

TABLE 4
Positional Parameters and Equivalent Isotropic *B* Factors for the Four Independent Atoms and Their Estimated Standard Deviations ($B_{eq}=\frac{4}{3}\sum\sum\beta_{ij}a_ia_j$)

	Atom	x	y	z	B_{eq} (Å^2)
$La_{0.84}Mo_6Se_8$	La	0	0	0	0.995(2)
	Mo	0.23515(3)	0.42227(3)	0.56144(3)	0.514(3)
	Se(1)	0.37859(5)	0.12049(5)	0.75307(5)	0.679(4)
	Se(2)	0.24166(5)	0.2417	0.2417	0.757(2)
$La_{0.88}Mo_6Se_8$	La	0	0	0	0.921(2)
	Mo	0.23535(4)	0.42250(4)	0.56163(4)	0.437(3)
	Se(1)	0.37848(5)	0.12040(5)	0.75313(5)	0.608(4)
	Se(2)	0.24212(5)	0.2421	0.2421	0.674(2)
$La_{0.94}Mo_6Se_8$	La	0	0	0	0.952(2)
	Mo	0.23561(4)	0.42262(4)	0.56194(4)	0.449(3)
	Se(1)	0.37846(5)	0.12023(5)	0.75314(5)	0.618(4)
	Se(2)	0.24255(5)	0.2425	0.2425	0.677(1)

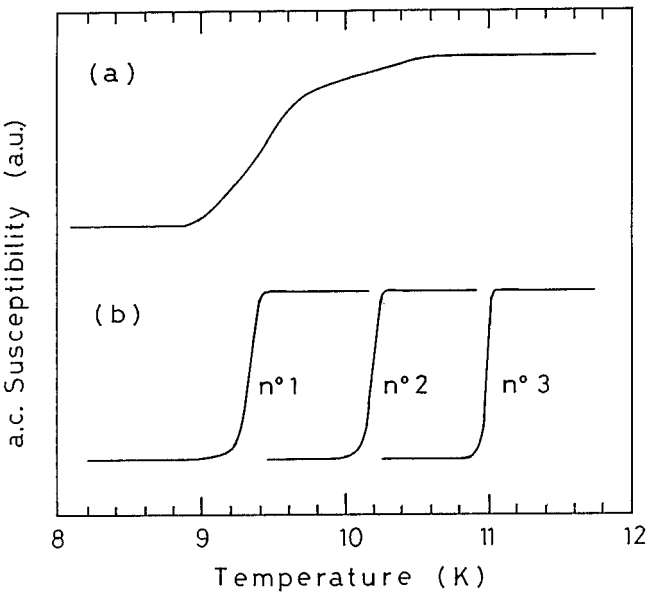

FIG. 2. In-phase ac susceptibility for four crystals of the $LaMo_6Se_8$ phase: (a) an average specimen showing a wide and multiple-step superconducting transition; (b) the three crystals chosen for structure refinement (T_c(no. 1) = 9.40(5) K; T_c(no. 2) = 10.25(5) K; T_c(no. 3) = 11.00(5) K).

lanthanum atom located at the origin is surrounded by eight selenium atoms belonging to eight different block units: it shares two short bondings (*RE*–Se(2)) with two selenium atoms Se(2) located on the ternary axis and six long bondings (*RE*–Se(1)) with selenium atoms occupying 6*f* positions. The lanthanum occupancy varied from sample to sample, going from $n(\mathrm{La}) = 0.84(1)$ to $n(\mathrm{La}) = 0.94(1)$, as will be thoroughly discussed shortly (see Table 3 and its corresponding footnote for a better estimation of the accuracy).

TABLE 5
Refined Temperature Factors and Their Estimated Standard Deviations[a]

	$\beta_{11}\times10^5$	$\beta_{22}\times10^5$	$\beta_{33}\times10^5$	$\beta_{12}\times10^5$	$\beta_{13}\times10^5$	$\beta_{23}\times10^5$
$La_{0.84}Mo_6Se_8$						
La	552(3)	β_{11}	β_{11}	−285(7)	β_{12}	β_{12}
Mo	279(3)	292(3)	275(3)	17(5)	11(5)	10(5)
Se(1)	285(4)	414(4)	414(4)	−35(6)	64(7)	122(7)
Se(2)	417(3)	β_{11}	β_{11}	−117(7)	β_{12}	β_{12}
$La_{0.88}Mo_6Se_8$						
La	511(3)	β_{11}	β_{11}	−265(7)	β_{12}	β_{12}
Mo	236(3)	230(3)	250(3)	24(5)	26(5)	10(5)
Se(1)	372(4)	250(4)	372(4)	−29(7)	120(7)	72(7)
Se(2)	372(3)	β_{11}	β_{11}	−127(7)	β_{12}	β_{12}
$La_{0.94}Mo_6Se_8$						
La	527(3)	β_{11}	β_{11}	−251(7)	β_{12}	β_{12}
Mo	244(3)	239(3)	253(3)	17(5)	17(5)	11(5)
Se(1)	379(4)	260(4)	369(4)	−24(7)	13(8)	74(7)
Se(2)	393(3)	β_{11}	β_{11}	−124(8)	β_{12}	β_{12}

[a] The thermal factor is given by $\exp\{-(\beta_{11}h^2+\beta_{22}k^2+\beta_{33}l^2+\beta_{12}hk+\beta_{13}hl+\beta_{23}kl)\}$.

3.2.2. Mo_6Se_8 Cluster Unit

Molybdenum–selenium distances. Each molybdenum atom, situated in a pyramidal environment, is bonded to one Se(2) atom located on the ternary axis (Mo–Se(2)) and to four Se(1) atoms, one of which belongs to an adjacent Mo_6Se_8 unit $((\mathrm{Mo–Se(1)})^{\mathrm{intra}}$ and $((\mathrm{Mo–Se(1)})^{\mathrm{inter}}$, respectively).

Molybdenum–molybdenum distances. Intracluster molybdenum–molybdenum distances are of two types: $(\mathrm{Mo–Mo})_{\Delta}^{\mathrm{intra}}$, between atoms situated on the same plane perpendicular to the ternary axis, and $(\mathrm{Mo}_{\Delta}–\mathrm{Mo}_{\Delta})^{\mathrm{intra}}$, between atoms situated on two neighboring planes (see Fig. 4). In the following, discussion will be mainly focused on the Mo–Mo distances since they are sensitive to charge transfer and stoichiometric effects.

The most significant intra- and intercluster distances deduced in this work are given in Table 6.

3.2.3. Anisotropic Thermal Vibrations

The thermal anisotropy of the lanthanum atoms was estimated at room temperature. In a model of full occupancy of the origin site, the lanthanum atoms undergo a harmonic motion; the root-mean-square displacements (RMSD) of these thermal vibrations are given by the perpendicular and parallel parameters $\langle X_{\perp}\rangle$ and $\langle X_{//}\rangle$, respectively, with respect to the ternary axis. For the three crystals

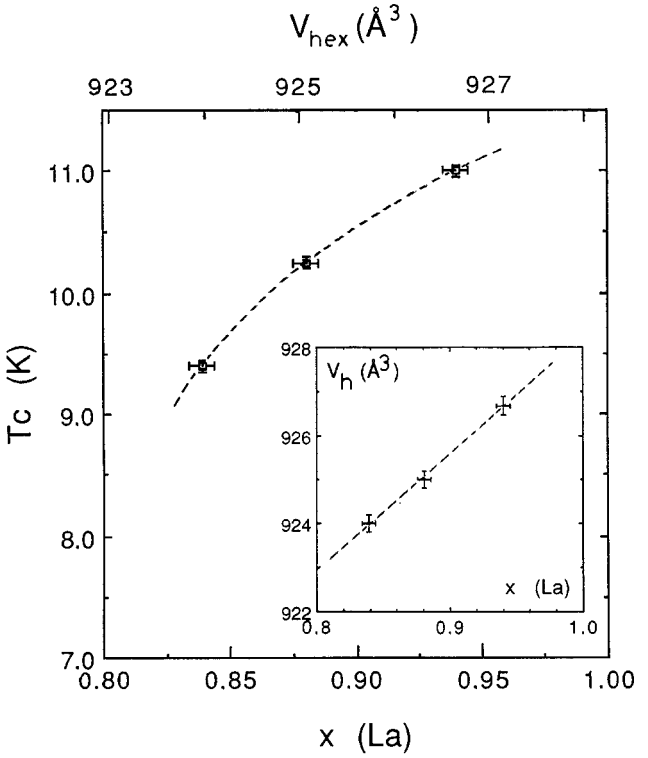

FIG. 3. Superconducting critical temperature as a function of (top) the cell volume V_H of the hexagonal lattice and (bottom) the lanthanum content x(La) for the three crystals presented in Fig. 2. The inset shows V_H versus x(La).

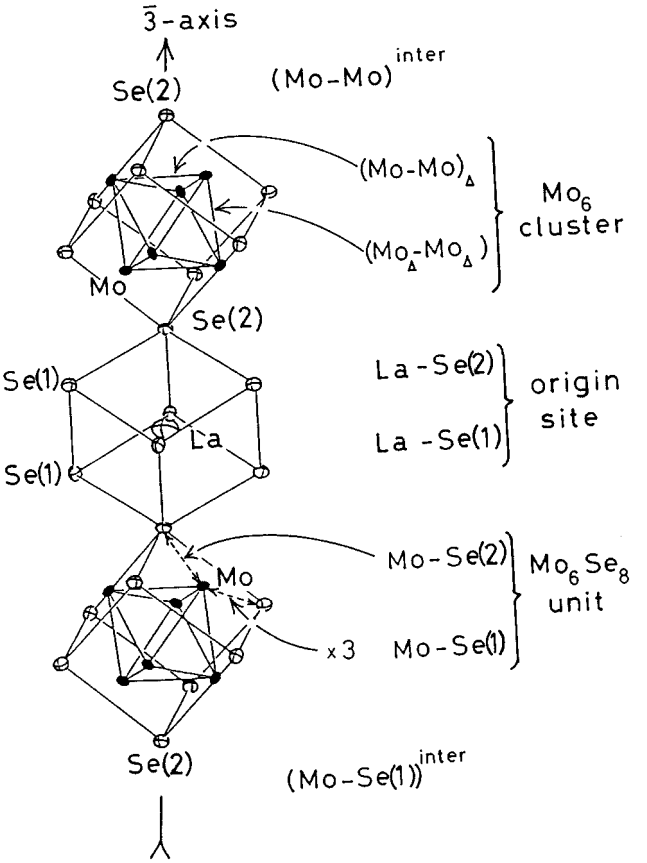

FIG. 4. Crystal structure of $LaMo_6Se_8$ defining some of the shortest interatomic distances. The $(X–Y)^{inter}$ distances relate the X atom of one cluster to the Y atom of the nearest cluster (see text).

studied in this work, $\langle X_{\perp} \rangle$ ranges between 0.120 and 0.125 Å, whereas $\langle X_{//} \rangle$ varies between 0.077 and 0.082 Å. These values are identical to those found for large rare-earth atoms in the well-known $RE Mo_6S_8$ series and confirm that there is no delocalization of the cation around the origin site [for comparison, the corresponding values for $CeMo_6S_8$ are 0.118 and 0.068 Å (11)].

4. DISCUSSION

4.1. T_c versus Lanthanum Occupancy

The structural results indicate that only the origin site is occupied by the lanthanum atoms. The lowest lanthanum stoichiometry in single crystals was found to be equal to 0.84(1), that is, at the lowest boundary of the Chevrel-phase domain. At the opposite side, the highest stoichiometry of lanthanum was found to be x(La) = 0.94(1), low compared to the maximum rare-earth content possible ($x(RE) = 1$) at the origin site. These results confirm that in the case of large cations, the rare-earth occupancy does not exceed 1 atom per unit cell, a situation already found in single crystals of $RE Mo_6S_8$ (11). This is worth mentioning since all the studies done in powder samples (see, for instance, ref 22) suggest a rare-earth content greater than unity. It should be recalled here that the only structure refinement of rare-earth molybdenum selenides published to date also gave a large deficiency in the rare-earth content ($La_{\sim 0.85}Mo_6Se_8$); however, this last result should be taken with extreme caution since the agreement factor was of the order of 10% (23).

As already pointed out, we were unable to find single crystals having a lanthanum content x(La) equal to 1. As shown in Fig. 3, which describes the critical temperature as a function of the lanthanum occupancy in the three crystals investigated in this study, the highest T_c observed was 11.0 K, that is, below the maximum value of 11.80(5) K found in polycrystalline samples (16, 17). This suggests that the lanthanum content did not reach the optimum value in any of the single crystals tested, a situation that seems to be encountered systematicallly for other rare earths (24), independent of our efforts to increase the rare-earth concentration. This is even more surprising in view of the case of the

TABLE 6
Shortest Interatomic Distances (Å) for $La_xMo_6Se_8$ Crystals

	$La_{0.84}Mo_6Se_8$	$La_{0.88}Mo_6Se_8$	$La_{0.94}Mo_6Se_8$
Mo_6 cluster			
$(Mo–Mo)_{\Delta}^{intra}$	2.6778(4)	2.6773(4)	2.6788(4)
$(Mo_{\Delta}–Mo_{\Delta})^{intra}$	2.7242(5)	2.7224(5)	2.7201(5)
$(Mo–Mo)^{inter}$	3.4370(4)	3.4400(5)	3.4458(5)
Mo_6Se_8 unit			
$(Mo–Se(1))^{intra}$	2.5648(4)	2.5660(4)	2.5667(4)
	2.5720(4)	2.5721(4)	2.5731(4)
	2.6374(4)	2.6376(4)	2.6399(4)
$(Mo–Se(1))^{inter}$	2.7210(4)	2.7238(4)	2.7264(5)
Mo–Se(2)	2.5042(4)	2.5038(3)	2.5040(3)
Origin site			
La–Se(1)	3.1340(3)	3.1330(3)	3.1341(4)
La–Se(2)	2.8919(2)	2.9014(2)	2.9093(2)

sulfides $RE Mo_6S_8$, where the upper limit ($x(RE) = 1.0$) was reached whenever the starting composition subjected to melting was enriched in binary rare-earth sulfides (10). However, a direct comparison of the single-crystal results with those obtained from polycrystalline samples should be done with caution. In fact, although the polycrystalline T_c data were collected at about 1200°C, the single crystals describe the $La_xMo_6Se_8$ line at a given cross section of the Chevrel-phase domain at temperatures higher than ~1620°C. At these high temperatures, the Chevrel-phase domain deviates toward a region which is less concentrated in lanthanum and becomes much narrower compared to the one found at 1200°C. An analogous case occurs in $Cu_xMo_6S_8$: according to ref 9, its domain of existence within the ternary system is also significantly shifted at high temperatures ($1.8 \leq x \leq 4$ at 800°C; $1.2 \leq x \leq 3$ at 1500°C).

Another possible explanation for the fact that our single crystals did not reach the maximum content of lanthanum comes from covalent bonding and ionic radii considerations for the chalcogen atoms. In fact, the chalcogen valence in such covalent bondings decreases from sulfur (−2) to selenium (−1.75) to tellurium (−1.33) (25), and, at the same time, the "degree of insertion" (that is, the quantity of metal that can fill the cationic sublattice) becomes much smaller (12). Charge transfer towards the Mo_6Se_8 network apparently scales down compared to the Mo_6S_8 case, and the conduction band fills much more quickly for selenium and tellurium than for sulfur compounds.

Because La has the largest ionic radius of the lanthanides, it should be noted that the lanthanum example is the most favorable case for observing such large variations in T_c; on the contrary, the critical temperature of Chevrel-phase selenides containing heavy rare-earth elements [e.g., $Ho_xMo_6Se_8$ (26)] is almost insensitive to the cationic concentration. This can be phenomenologically explained by the T_c dependence of the $RE Mo_6X_8$ (X = S, Se) series as a function of the ionic radius of the rare-earth atom (27). Band structure calculations are in progress to explain this dependence, not only in the Chevrel-phase series but also in the recently discovered lanthanide-doped solid solutions of the Mo_3Se_4 binary (28).

4.2. Interatomic Distances versus Lanthanum Occupancy

Figure 5 shows the intercluster distances [$(Mo–Mo)^{inter}$ and $(Mo–Se(1))^{inter}$] as a function of the lanthanum occupancy. Their systematic increase with growing lanthanum content implies that the Mo_6Se_8 block units are situated further apart when the occupation of the origin site increases.

Figure 6 shows the average distances prevalent within the pseudocubic origin site, namely the La–Se(1) and La–Se(2) distances. Due to the different lanthanum occupancies, these distances just reflect the average value measured in the ensemble of sites for a given crystal. With this in mind, Fig. 6 indicates that the origin site elongates along the axial direction, as evidenced by the increase of the La–Se(2) bondings, whereas the six longer La–Se(1) distances between the cation and the 6*f* selenium positions remain unchanged.

The size of the molybdenum cluster is mainly sensitive to charge transfer effects, that is to a variation of the overall valence of the lanthanum sublattice: the Mo–Mo distance between two neighboring planes perpendicular to the ternary axis [$(Mo_{\Delta}–Mo_{\Delta})^{intra}$] decreases when the lanthanum

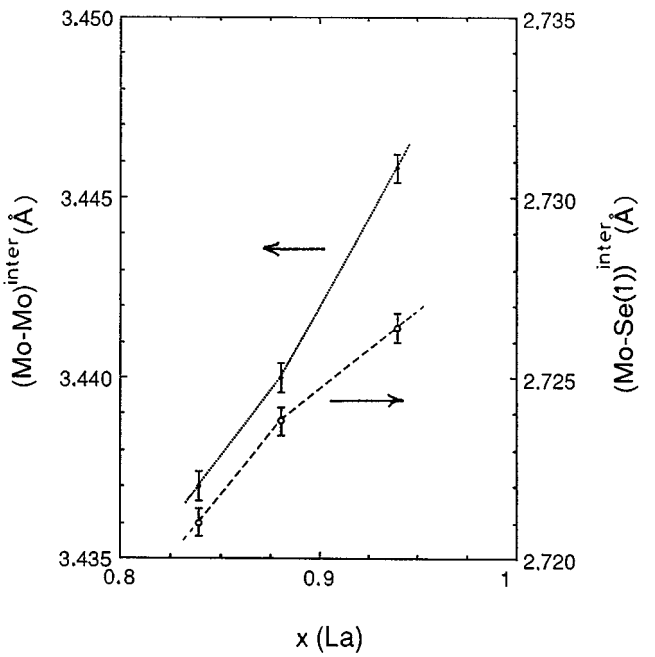

FIG. 5. Intercluster distances as a function of the lanthanum occupancy (error bars represent the estimated standard deviations (esd's) given in Table 6).

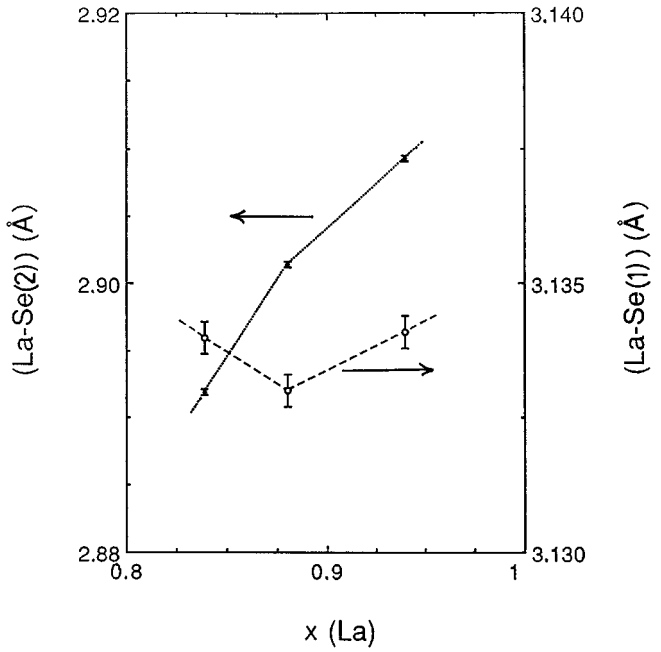

FIG. 6. Average La–Se distances prevalent in the pseudocubic origin site (see Fig. 4) as a function of the lanthanum occupancy (error bars represent the esd's).

concentration increases, whereas the distance inside each plane [$(\text{Mo–Mo})_{\Delta}^{\text{intra}}$] remains constant (Fig. 7). Thus the cluster contracts when a more effective charge transfer from the lanthanum sublattice toward the molybdenum cluster takes place. This phenomenon is common to all Chevrel phases and is due to a decrease of the molybdenum oxidation state within the Mo_6 cluster (12).

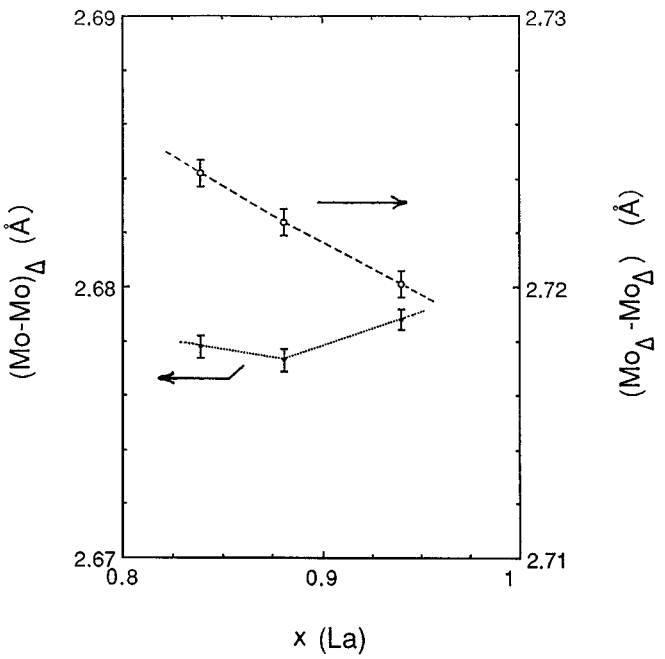

FIG. 7. Intracluster Mo–Mo distances, as defined in Fig. 4, as a function of the lanthanum occupancy (error bars represent the esd's).

All other intracluster distances Mo–Se(2) and Mo–Se(1) stay fairly constant with respect to the lanthanum occupancy, within the limits of our experimental accuracy (Table 6).

It should be noted that the cluster's size variation goes in the opposite way to the variation of the intercluster distances $(\text{Mo–Se(1)})^{\text{inter}}$ and $(\text{Mo–Mo})^{\text{inter}}$, partly compensating the overall increase of the unit cell. However, because of the large size of the lanthanum ion, the origin site (Fig. 6) increases by one order of magnitude more than the corresponding contraction of the Mo_6 cluster. To a lesser extent, the intercluster distances (Fig. 5) increase faster than the $(\text{Mo}_{\Delta}–\text{Mo}_{\Delta})$ bondings decrease (Fig. 7).

As a result, there is a significant increase of the unit cell parameters when the concentration of lanthanum increases (inset, Fig. 3). For smaller rare-earth ions (the case of $Ho_xMo_6S_8$ discussed in ref 29), the increase of the pseudocubic origin site was fully compensated by the decrease of the cluster's size, all other distances staying almost constant when the concentration of holmium was changed, leading to an overall decrease of the cell parameters ($V_{\text{hex}} = 807.8$ and 804.0 Å^3, for $x = 0.88$ and 1.0, respectively). A parallel study is being undertaken in the system $La_xMo_6S_8$ to compare the interatomic distances and the lattice parameters as a function of both the size of the rare-earth cation and the oxidation state of the chalcogen anion.

5. CONCLUSION

Single crystals of the superconducting Chevrel-phase lanthanum molybdenum selenide $LaMo_6Se_8$ were grown. The critical temperature T_c was found to be sample dependent, ranging between 9.4 and 11.0 K.

To our knowledge, with the exception of $La_{\sim 0.85}Mo_6Se_8$, poorly refined as shown by an R factor of 10% (23), no other structural refinement has been previously carried out on rare-earth-based Chevrel-phase selenides. In this work, we have presented a crystal structure analysis of the $La_xMo_6Se_8$ phase based on the study of three single crystals having different contents x of lanthanum. The structure belonged to the series of "large cations" (12) and was identical to the well-known structures of $PbMo_6S_8$ or $REMo_6S_8$. Refinement of the occupancy of the origin site by the lanthanum cation led to an unambiguous correlation between the critical temperature T_c and the rare-earth concentration x(La).

Interatomic distances have been presented as a function of the lanthanum content. They show that the size of the origin site at the center of the pseudocubic Se_8 unit is the most important parameter fixing the unit cell constants, at

least for the largest lanthanides. Also, the intercluster distances increase at the same time as the unit cell, which have important consequences on the transport and superconducting properties (18). On the other hand, the intracluster distances depend mostly on charge transfer effects: with increasing cationic concentration, a slight contraction of the Mo_6 cluster occurs, due to a decrease of the oxidation state of the molybdenum atom.

The present report is complemented with results on the transport, magnetic, and superconducting properties obtained in these crystals [accompanying paper, this issue (18)]. It will be also extended to other lanthanides, mainly to those that present a re-entrant behavior into a low-temperature magnetically ordered state (RE = Ho, Gd, Er, etc.). Ambiguous results obtained in sintered materials might now be solved in single crystals where no superconducting secondary phase Mo_3Se_4 is present.

ACKNOWLEDGMENTS

We are grateful to Dr. M. Potel for acquiring all the data for the crystal structure refinement and to J.-C. Jegaden for SEM analysis.

REFERENCES

1. Ø. Fischer, A. Treyvaud, R. Chevrel, and M. Sergent, *Solid State Commun.* **17,** 721 (1975).
2. R. N. Shelton, R. W. McCallum, and H. Adrian, *Phys. Lett. A* **56,** 213 (1976).
3. B. T. Matthias, E. Corenzwit, J. M. Vandenbert, and H. Barz, *Proc. Natl. Acad. Sci. U.S.A.* **74,** 1334 (1977).
4. J. C. Ho, P. H. Hor, R. L. Meng, C. W. Chu, and C. Y. Huang, *Solid State Commun.* **63,** 711 (1987).
5. B. D. Dunlap, M. Slaski, D. G. Hinks, L. Soderholm, M. Beno, K. Zhang, C. Segre, G. W. Crabtree, W. K. Kwok, S. K. Malik, I. K. Schuller, J. D. Jorgensen, and Z. Sungaila, *J. Magn. Magn. Mater.* **68,** L-139 (1987).
6. M. B. Maple, N. Y. Ayoub, T. Bjørnholm, E. A. Early, S. Ghamaty, B. W. Lee, J. T. Markert, J. J. Neumeier, and C. L. Seaman, *Physica C* **162–164,** 296 (1989).
7. R. Nagarajan, C. Mazumdar, Z. Hossain, S. K. Dhar, K. V. Gopalakrishnan, L. C. Gupta, C. Godart, B. D. Padalia, and R. Vijayaraghavan, *Phys. Rev. Lett.* **72,** 274 (1994).
8. R. J. Cava, H. Takagi, B. Batlogg, H. W. Zandbergen, J. J. Krajewski, W. F. Beck, Jr., T. Siegrist, K. Mizuhashi, J. O. Lee, H. Eisaki, and S. Uchida, *Nature* (*London*) **367,** 252 (1994).
9. R. Flükiger, *in* "Superconductor Materials Science, Series B" (S. Foner and B. Schwartz, Eds.), Chap. 8, pp. 511–604. Plenum, New York, 1981.
10. R. Horyń, O. Peña, C. Geantet, and M. Sergent, *Supercond. Sci. Technol.* **2,** 71 (1989).
11. O. Peña and M. Sergent, *Prog. Solid State Chem.* **19,** 165 (1989).
12. R. Chevrel and M. Sergent, *in* "Topics in Current Physics: Superconductivity in Ternary Compounds I" (Ø. Fischer and M. B. Maple, Eds.), Vol. 32, Chap. 2, pp. 25–86. Springer-Verlag, Berlin, Heidelberg, New York, 1982.
13. R. Horyń, O. Peña, A. Wojakowski, and M. Sergent, *Supercond. Sci. Technol.* **7,** 146 (1994).
14. O. Peña, F. Le Berre, M. Sergent, R. Horyń, and A. Wojakowski, *Physica C* **235–240,** 771 (1994).
15. F. Maho, F. Le Berre, O. Peña, R. Horyń, and A. Wojakowski, *J. Phys. III Fr.* **5,** 1 (1995).
16. F. Le Berre, O. Peña, M. Sergent, R. Horyń, and A. Wojakowski, Proc. Vth Eur. Conf. Solid State Chem., Montpellier, France, Sept. 4–7, 1995; R. Horyń, F. Le Berre, A. Wojakowski, and O. Peña, *Supercond. Sci. Technol.* **9,** 1081 (1996).
17. R. Horyń, A. Wojakowski, F. Le Berre, and O. Peña, Proc. 1st Polish–U.S. Conf. High-T_c Supercond., Wroclaw, Poland, Sept. 11–15, 1995 (unpublished).
18. O. Peña, F. Le Berre, J. Padiou, T. Marchand, R. Horyń, and A. Wojakowski, *J. Solid State Chem.* **136,** 160 (1998).
19. P. Coppens, L. Leiserowitz, and D. Rabinovich, *Acta Crystallogr.* **18,** 1035 (1965).
20. J. Guillevic, H. Le Strat, and D. Grandjean, *Acta Crystallogr., Sect. B* **32,** 1342 (1976).
21. O. Peña, P. Gougeon, M. Sergent, and R. Horyń, *J. Less-Common Met.* **99,** 225 (1984).
22. "Topics in Current Physics: Superconductivity in Ternary Compounds I" (Ø. Fischer and M. B. Maple, Eds.), Vol. 32. Springer-Verlag, Berlin, Heidelberg, New York, 1982; "Topics in Current Physics: Superconductivity in Ternary Compounds II" (M. B. Maple and Ø. Fischer, Eds.), Vol. 34. Springer-Verlag, Berlin, Heidelberg, New York, 1982.
23. K. Yvon, *in* "Current Topics in Materials Science" (E. Kaldis, Ed.), Vol. 3, pp. 53–129. North-Holland, Amsterdam, 1979.
24. F. Le Berre, Thesis, University of Rennes I, 1996; F. Le Berre *et al.*, to be published.
25. M. Sergent, Ø. Fischer, M. Decroux, C. Perrin, and R. Chevrel, *J. Solid State Chem.* **22,** 87 (1977).
26. F. Le Berre, F. Maho, O. Peña, R. Horyń, and A. Wojakowski, *J. Magn. Magn. Mater.* **140–144,** 1171 (1995).
27. F. Le Berre, O. Peña, and M. Sergent, to be published.
28. F. Le Berre, D. Tshimanga, A. L. Guilloux, J. Leclercq, M. Sergent, O. Peña, R. Horyń, and A. Wojakowski, *Physica B* **228,** 261 (1996).
29. O. Peña, R. Horyń, M. Potel, J. Padiou, and M. Sergent, *J. Less-Common Met.* **105,** 105 (1985).